THE JOURNAL OF PHYSICAL CHEMISTRY C

Article

pubs.acs.org/JPCC

Microstructural Thermal Evolution of the Na_2CO_3 Phase Produced during a Na_2ZrO_3–CO_2 Chemisorption Process

Lorena Martínez-dlCruz and Heriberto Pfeiffer*

Instituto de Investigaciones en Materiales, Universidad Nacional Autónoma de México, Circuito exterior s/n, Ciudad Universitaria, Del. Coyoacán, CP 04510,México DF, Mexico

ABSTRACT: Na_2ZrO_3 was synthesized by a solid-state reaction, and a CO_2 chemisorption process was evaluated as a function of temperature to determine whether structural and/or microstructural modifications occurred during the reaction process. This study was performed using the following techniques: thermogravimetry, X-ray diffraction, scanning and transmission electron microscopy, and N_2 adsorption. The results clearly show that Na_2CO_3–ZrO_2 was produced on the external shell of Na_2ZrO_3 during the CO_2 chemisorption process. The microstructural properties varied as a function of temperature. The Na_2ZrO_3–CO_2 chemisorption reaction was not limited at $T \leq 550$ °C because the Na_2CO_3–ZrO_2 external shell contained mesopores. CO_2 diffused through the mesoporous shell, and the reaction continued. Conversely, if the CO_2 chemisorption occurred at $T > 550$ °C, the mesoporosity on the Na_2CO_3–ZrO_2 external shell was not observed, and the chemisorption was kinetically controlled by the diffusion of CO_2 through the sodium crystal phases.

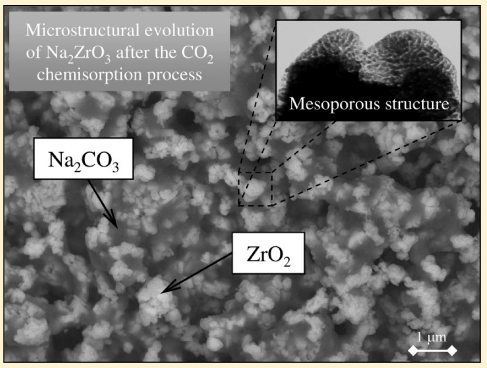

INTRODUCTION

In the past two decades, several materials have been proposed as potential CO_2 captors.[1−6] Among the different materials studied in this field, some alkaline (lithium and sodium) ceramics seem to have several interesting properties for the capture of CO_2 at high temperatures.[1,3,7−37] The most highly studied alkaline ceramics are Li_4SiO_4, Li_5AlO_4, Li_2ZrO_3, and Na_2ZrO_3.[7−37]

In general, it has been accepted that all these alkaline ceramics capture CO_2 through the following reaction mechanism. Initially, at low temperatures, there is a CO_2 chemisorption over the surface of the ceramic, which implies that an external shell is formed that is composed of the corresponding alkaline carbonate (Na_2CO_3 or Li_2CO_3). Occasionally, other secondary phases are observed. When the entire ceramic surface has reacted, the superficial CO_2 chemisorption is complete. The CO_2 chemisorption can be reactivated if the temperature is increased sufficiently to allow diffusion processes and the reaction to continue throughout the bulk of the material.[38] Reports in the literature indicate that isothermal CO_2 chemisorptions sometimes follow atypical behaviors. In the first temperature range, the CO_2 chemisorption increases as a function of temperature, as expected. Then, in the intermediate temperature range, the CO_2 chemisorption will dramatically decrease, resulting in even lower CO_2 capture than those observed at the lowest temperatures. Finally, at higher temperatures, CO_2 chemisorption is reactivated and increases as a function of temperature.[17,28,35] The decrease has been associated with a sintering process of the ceramic powder, which produces an important decrement of the surface area, which inhibits the initial superficial reaction. Subsequently, as the diffusion processes are activated, sintering and surface area are no longer the preponderant factors, and the CO_2 chemisorption is recovered. However, this statement has not been experimentally analyzed and probed.

On the other hand, Na_2ZrO_3 and other sodium containing phases have not been thoroughly studied as CO_2 chemisorbents, although they possess interesting properties.[11,20−25,27] López-Ortiz and co-workers[21] were the first authors to show that Na_2ZrO_3 was able to chemisorb CO_2. Subsequently, a few additional papers were published that showed some results regarding CO_2 absorption on Na_2ZrO_3.[23−25,27] Perhaps, the most important property of the CO_2 chemisorption on Na_2ZrO_3 is the fact that this reaction occurs over a wide temperature range, i.e., room temperature to 850 °C. Additionally, Na_2ZrO_3 follows the same atypical behavior during the isothermal CO_2 chemisorption process as described above.[23]

Therefore, the aim of the present work was to analyze the microstructural properties of the Na_2ZrO_3 ceramic powders after the CO_2 chemisorption process occurred at different temperatures to elucidate any differences that could explain the CO_2 chemisorption mechanism and the atypical isothermal behavior described in previous papers. Na_2ZrO_3 was selected as the absorbent for the study because Na_2ZrO_3 has a considerably high CO_2 chemisorption, and the chemisorption occurs over a wide temperature range.

Received: February 27, 2012
Revised: April 10, 2012
Published: April 10, 2012

EXPERIMENTAL SECTION

Na_2ZrO_3 was synthesized using a solid-state reaction that employed sodium carbonate (Na_2CO_3, Aldrich) and zirconium oxide (ZrO_2, Aldrich). The powders were mechanically mixed and heated at 850 °C for 6 h. To obtain pure Na_2ZrO_3, 20 wt % excess sodium carbonate was used due to the tendency of sodium carbonate to sublimate.

A diffractometer (Bruker AXS, D8 Advance) coupled to a copper anode X-ray tube was used to identify the phases obtained during the synthesis and after the CO_2 capture process. Na_2ZrO_3 was identified by the corresponding Joint Committee Powder Diffraction Standards (JCPDS). Nitrogen adsorption−desorption isotherms were acquired using the Bel-Japan Minisorp II instrument at 77 K using a multipoint technique. Samples were degassed at room temperature for 12 h in vacuum prior to analysis. The morphology of the Na_2ZrO_3 material was analyzed with scanning (SEM, JEOL JMS-7600F) and transmission (TEM, JEOL JEM-1200EX) electron microscopes.

The CO_2 chemisorption isotherms were performed using a Q500HR instrument (TA Instruments). Samples were initially heated to the corresponding temperature (between 300 and 750 °C) under a N_2 flow. As the sample reached the corresponding temperature, the gas flow was switched from N_2 to CO_2. The isothermal experiments were performed using a gas flow rate of 60 mL/min (Praxair, grade 3.0) throughout the duration of the experiment. Finally, to elucidate the mechanism of CO_2 capture by the Na_2ZrO_3 and the corresponding microstructural properties, the samples obtained from the isothermal analyses (Na_2ZrO_3−CO_2 sample products) were recharacterized by X-ray diffraction (XRD), SEM, TEM and N_2 adsorption.

RESULTS AND DISCUSSION

Characterization of the Na_2ZrO_3 Sample. Na_2ZrO_3 was synthesized by a solid-state reaction, and the XRD pattern is shown in Figure 1. The diffraction pattern was perfectly fit to the JCPDS file 35-0770, which corresponds to the Na_2ZrO_3 phase with a monoclinic structure. Therefore, Na_2ZrO_3 was obtained without the presence of any impurity, at least at the XRD detection level.

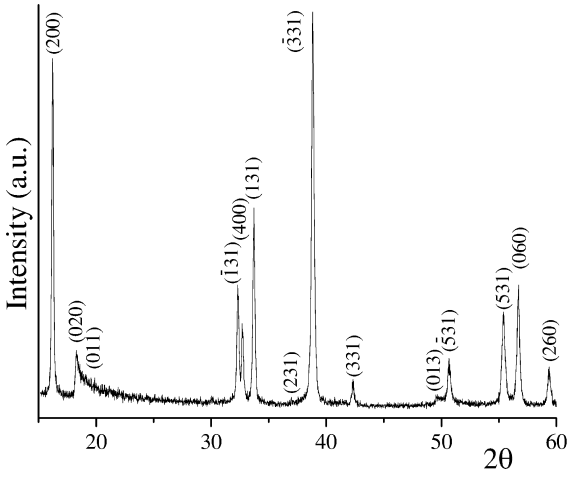

Figure 1. XRD pattern of the Na_2ZrO_3 synthesized by the solid-state reaction. The diffraction peaks were fit to the JCPDS file 35-0770, which corresponded to the Na_2ZrO_3 monoclinic phase.

Then, microstructural properties of the Na_2ZrO_3 sample were determined by SEM (morphology and particle size) and N_2 adsorption (surface area and pore diameter). Figure 2 shows

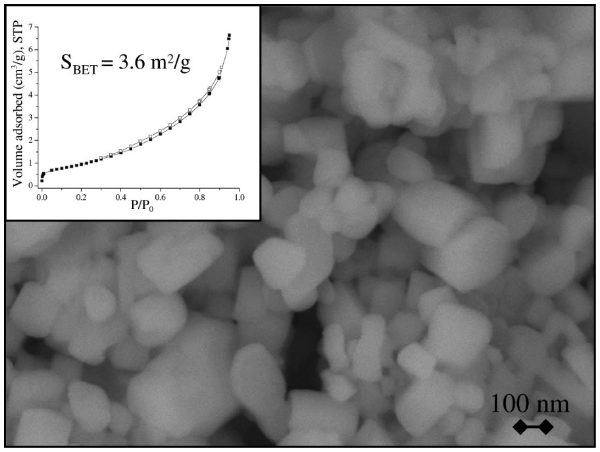

Figure 2. SEM image of the Na_2ZrO_3 synthesized by the solid-state reaction. The square inset shows the N_2 adsorption−desorption isotherm of the sample.

that Na_2ZrO_3 particles had a dense polyhedral morphology with particle sizes between 150 and 400 nm. These particles produced large agglomerates of approximately 10 μm. In fact, the dense morphology was corroborated by the surface analysis. The square inset of Figure 2 shows the N_2 adsorption−desorption isotherm of the Na_2ZrO_3 sample. The curve corresponds to a type II isotherm, which exhibits a very narrow H3-type hysteresis loop according to the IUPAC classification.[39,40] This behavior corresponds to nonporous, dense aggregate particles. The surface area obtained was very small (3.6 m^2/g).

Kinetic Analysis of the CO_2 Absorption. Previously, Na_2ZrO_3 was reported to be able to chemisorb CO_2 over a wide temperature range (room temperature to approximately 850 °C).[23−25,27] Usually, there is an initial CO_2 superficial chemisorption between room temperature and 300 °C. Then, the CO_2 capture process is reactivated at temperatures higher than 400 °C, and it is associated with the CO_2 chemisorption process controlled by diffusion processes. On the basis of this information, several isothermal experiments were performed between 150 and 750 °C (Figure 3). Initially, the isothermic experiments performed at 150 and 200 °C showed exponential behaviors, where the equilibrium were not reached. In these cases, the maximum CO_2 chemisorption values were 8.4 and 10.3 wt % at 150 and 200 °C, respectively, after 180 min of reaction. However, when the isotherm was performed at 300 °C, the total chemisorption was decreased to 7 wt % in the same period of time. The decrement observed in this low temperature range has been associated with a sintering effect of the initial Na_2ZrO_3 phase.[23] Later, a similar exponential behavior was obtained in the samples treated at 400 and 500 °C, which had significantly increased the CO_2 chemisorption (17.6 and 18.2 wt %, respectively). The sample treated at 550 °C presented the highest CO_2 chemisorption (23.8 wt %). In fact, the whole CO_2 chemisorption occurred in approximately 10 min, corresponding to a final reaction efficiency of 100%, as the theoretical maximum CO_2 chemisorption on Na_2ZrO_3 is equal to 23.8 wt %.

dx.doi.org/10.1021/jp301917a | J. Phys. Chem. C 2012, 116, 9675−9680

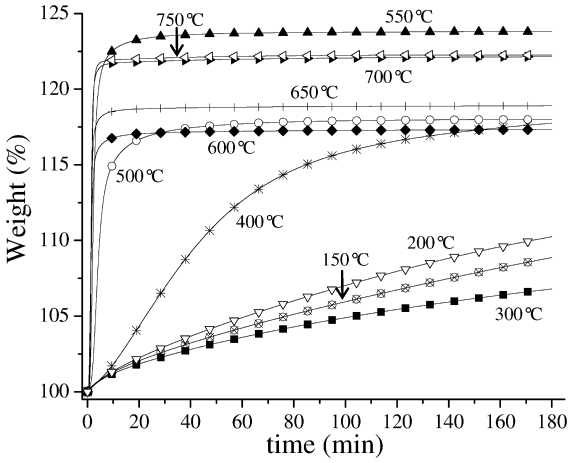

Figure 3. CO_2 chemisorption isotherms performed on Na_2ZrO_3 at different temperatures.

When the sample was isothermically treated at 600 °C or higher temperatures, it resulted in a decrease in the CO_2 chemisorption. Therefore, less CO_2 was chemisorbed at $T >$ 550 °C than that chemisorbed at 550 °C. This atypical phenomenon, presented at high temperatures, has been observed in some lithium ceramics, and it has been associated with the sintering process of the samples.[17,28] but has not been thoroughly studied. In addition, in the Na_2ZrO_3 case, the sintering process had already been presented at around 300 °C. Finally, between 600 and 750 °C, the diffusion processes are activated, and therefore the CO_2 chemisorption is recovered, increasing as a function of temperature. Nevertheless, it must be mentioned that, although the CO_2 chemisorption increased as a function of temperature (in the last samples), the maximum CO_2 chemisorption was obtained at 550 °C.

Structural and Microstructural Analyses of the Na_2ZrO_3–CO_2 Isothermal Products. To further analyze and understand the CO_2 chemisorption on Na_2ZrO_3 and the resultant effects, some of the Na_2ZrO_3–CO_2 isothermal products were recharacterized by XRD, N_2 adsorption, SEM, and TEM.

Initially, the Na_2ZrO_3–CO_2 isothermal products were analyzed by XRD (Figure 4). As shown, the presence of Na_2CO_3 was observed in the sample treated at 300 °C, which simply corresponds to the main product obtained during the CO_2 chemisorption on Na_2ZrO_3. As expected, increasing the temperature during the isothermal procedures caused an increase in the amounts of Na_2CO_3 and ZrO_2 phases, while the Na_2ZrO_3 tended to disappear. Notably, as can be observed from these XRD patterns, the Na_2CO_3 crystal size increased as a function of the temperature. While the Na_2CO_3 crystal size obtained at 500 °C was 104 Å, the size increased to 379 Å on the sample treated at 750 °C (Table 1). These results indicate that some microstructural properties of the product's external shell are being modified as a function of temperature. These results are in good agreement with the atypical behavior observed in the CO_2 isothermal analysis and are attributed to a sintering process.

After the structural characterization of the Na_2ZrO_3–CO_2 isothermal products, different microstructural aspects were analyzed by N_2 adsorption, SEM, and TEM. Figure 5 shows the N_2 adsorption–desorption isotherms of some of the Na_2ZrO_3–CO_2 isothermal products, which clearly show different textural properties for all the samples. Even though the Na_2ZrO_3 sample

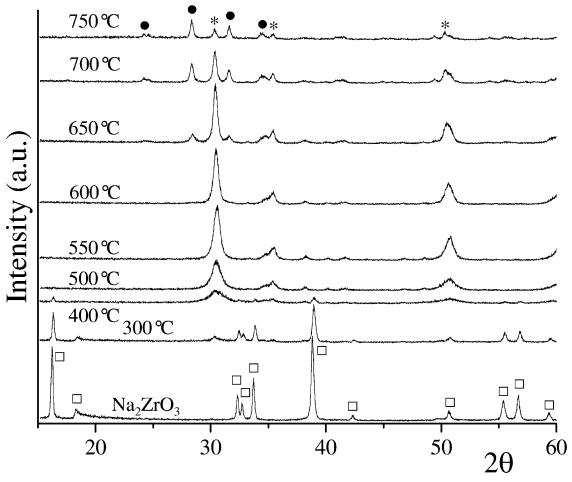

Figure 4. XRD patterns of the Na_2ZrO_3–CO_2 sample products obtained from the different isothermal experiments. The peaks were labeled as follows: □ Na_2ZrO_3, ● ZrO_2, and ∗ Na_2CO_3.

Table 1. Microstructural Properties of the Na_2ZrO_3–CO_2 Sample Products Determined by XRD and N_2 Adsorption

CO_2 temp. chemisorption (°C)	Na_2CO_3 crystal size (Å)	S_{BET} (m^2/g)	r_{porous} (nm)
original		3.6	1.9
300		3.2	1.9
400		3.0	2.1
500	104	34.0	1.9
550	130	21.0	3.1
600	178	3.4	2.1
650	214	2.5	1.9
750	379		

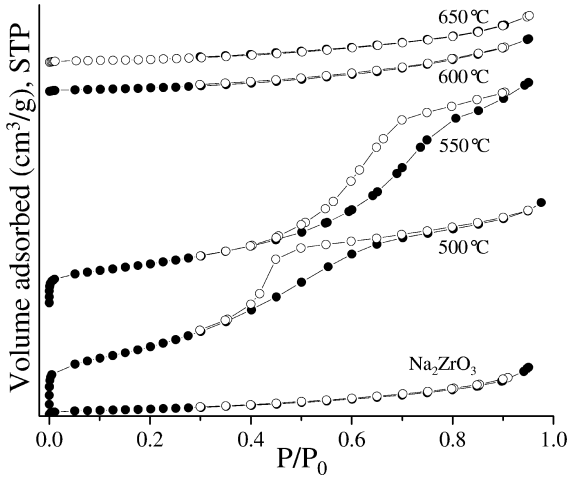

Figure 5. N_2 adsorption–desorption isotherms of the Na_2ZrO_3–CO_2 sample products obtained from different isothermal experiments.

presented type II isothermal behavior, treatment of the sample at 500 and 550 °C resulted in type IV isotherms and H3 hysteresis loops.[39] These isotherm behaviors correspond to mesoporous materials. The surface areas increased in comparison to the original Na_2ZrO_3 sample (3.6 m^2/g). The surface areas obtained on the Na_2ZrO_3 samples treated at 500 and 550 °C were 34.0 and 21.0 m^2/g, respectively (Table 1). Thus, the pore diameters of the 500 and 550 °C heat-treated samples could be fully determined using the Barrett–Joyner–

dx.doi.org/10.1021/jp301917a | J. Phys. Chem. C 2012, 116, 9675–9680

Halenda (BJH) method. The obtained values were 3.8 and 6.2 nm, respectively (Figure 6). Therefore, the porosity and surface

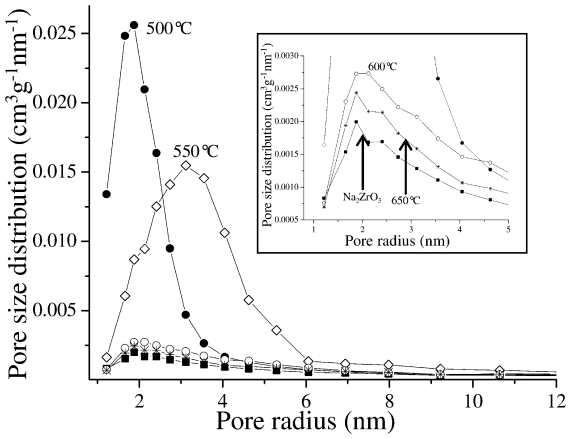

Figure 6. BJH pore size distributions derived from the N_2 adsorption isotherms performed on the Na_2ZrO_3–CO_2 sample products obtained from different isothermal experiments.

area increments were produced by the Na_2CO_3 external shell. However, when the Na_2ZrO_3 sample was treated at temperatures of 600 °C or higher, the N_2 adsorption isotherms returned to being type II, and the hysteresis loops tended to disappear, as was observed for the original Na_2ZrO_3 sample. The surface areas became as small as those determined in the original Na_2ZrO_3 sample, and the porosity practically disappeared (Table 1). These results confirmed the sintering process proposed in previous papers.[17,28] In previous studies, the sintering process had usually been attributed to the alkaline ceramic, not to the carbonate external shell; the opposite seems to be true in this case.

Figures 7 and 8 shows the SEM and TEM images obtained from the Na_2ZrO_3–CO_2 isothermal product treated at 550 °C.

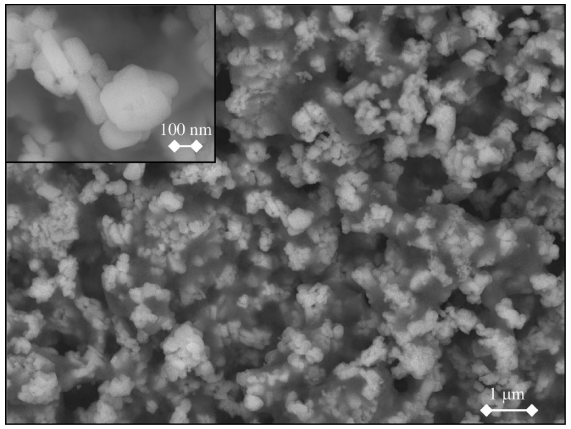

Figure 7. BSEI of the Na_2ZrO_3–CO_2 sample product isothermally treated at 550 °C.

The backscattered electron image (BSEI) in Figure 7 confirms the presence of two phases in the surface region. These two phases are most likely Na_2CO_3 and ZrO_2 because they are the Na_2ZrO_3 carbonation products. According to the isothermal data, this sample presented the highest efficiency (100%), so the Na_2ZrO_3 phase had disappeared. Therefore, the difference in contrast observed in Figure 7 must arise from the differences

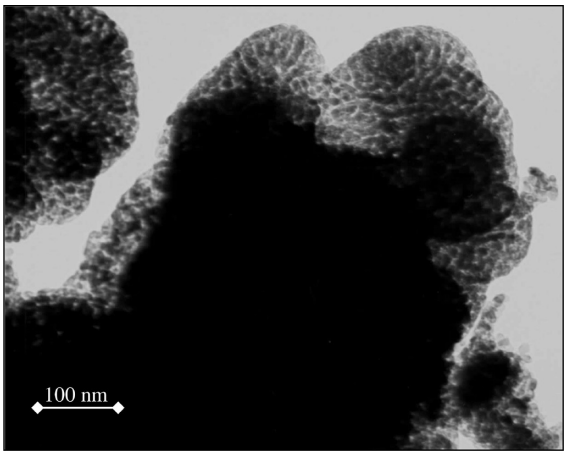

Figure 8. Bright-field TEM image of the Na_2ZrO_3–CO_2 sample product isothermically treated at 550 °C.

in mean atomic number, $\bar{Z}$, of Na_2CO_3 ($\bar{Z}$ = 8.666) and ZrO_2 ($\bar{Z}$ = 18.666), which led to a difference in the backscattered electron coefficient, η, of the two phases.[41] η increases from 0.0999 for Na_2CO_3 (the darker phase in Figure 7) to 0.2145 for ZrO_2 (the lighter phase). Moreover, the particle size does not seem to have changed, although the lighter particles (ZrO_2) seem to be interconnected or wrapped through the darker phase (Na_2CO_3). Interestingly, the particle surfaces appear to be corrugated, although the original Na_2ZrO_3 particles possessed very flat surfaces.

To further understand the microstructure, the same Na_2ZrO_3–CO_2 isothermal product treated at 550 °C was analyzed by TEM. Figure 8 shows the bright-field image of one these particles, where it is clearly evident that very tiny particles of approximately 10 nm are present. In fact, the values are in good agreement with the crystal sizes determined by XRD. Additionally, the surface agglomeration of these particles was most likely responsible for the mesoporosity detected and the surface particle corrugation observed by N_2 adsorption and SEM, respectively.

Figure 9 shows the BSEI of the Na_2ZrO_3–CO_2 isothermal product treated at 750 °C. As it was observed in the sample heat treated at 550 °C, the two phases are still present in this sample and correspond to Na_2CO_3 and ZrO_2. However, the particle sizes decreased considerably (approximately 100 nm)

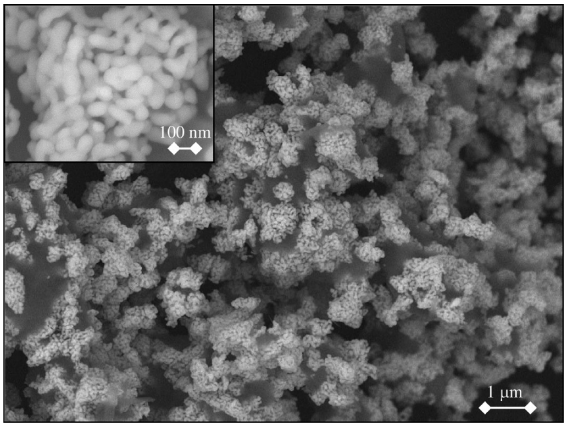

Figure 9. BSEI of the Na_2ZrO_3–CO_2 sample product isothermically treated at 750 °C.

dx.doi.org/10.1021/jp301917a | J. Phys. Chem. C 2012, 116, 9675–9680

compared to the particle sizes detected on the sample treated at 550 °C (150−400 nm). However, when the TEM analysis was performed on this sample, the very tiny particles of 10 nm disappeared. Only large, dense particles were observed (data not shown). The surface area and porosity decreased and tended to disappear (see N_2 adsorption−desorption experiments). Hence, the smallest particles (10 nm) probably sintered and grew to produce these new 100 nm particles detected on the last SEM image.

On the basis of all these results and previous reports, the CO_2 capture on Na_2ZrO_3 depends on different factors, which are shown as a scheme in Figure 10. At temperatures ≤550 °C

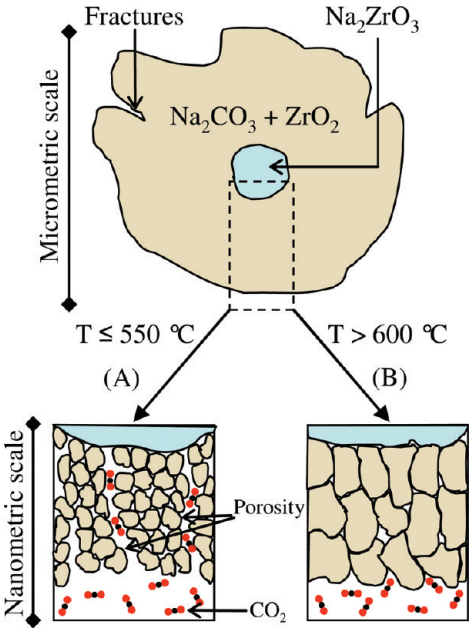

Figure 10. Scheme of the CO_2 chemisorption on Na_2ZrO_3 at different temperatures. (A) $T \leq 550$ °C; the Na_2CO_3−ZrO_2 external shell is mesoporous, and the CO_2 diffusion occurs through the mesoporous structure. (B) $T > 550$ °C; the Na_2CO_3−ZrO_2 external shell is not porous.

(Figure 10A), the Na_2CO_3 and ZrO_2 external shell, produced over the Na_2ZrO_3 particles, contains mesopores produced by the presence of very tiny particles (~10 nm) over the ceramic surfaces. Therefore, the presence of these types of pores in the external shell allowed CO_2 diffusion to occur, and, consequently, the Na_2ZrO_3−CO_2 reaction continued. However, at temperatures higher than 550 °C, the Na_2CO_3 and ZrO_2 external shells probably sinter, and the porosity disappears (Figure 10B). In this case, CO_2 is not able to diffuse through the external shell. Therefore, the CO_2 chemisorption must be controlled by the sodium ionic diffusion through the Na_2CO_3 crystals. Furthermore, XRD and microscopic analyses showed that Na_2CO_3−ZrO_2 crystals and particle sizes increased concomitantly with temperature. As is illustrated in Figure 10, the crystal and particle sizes of the external shells were different at each temperature range. This confirms the sintering effect produced on the material, and therefore the sodium diffusion process may become the limiting step of the whole CO_2 chemisorption process on Na_2ZrO_3.

CONCLUSIONS

Na_2ZrO_3 was synthesized by a solid-state reaction, and the CO_2 chemisorption process was evaluated as a function of temperature. Structural and microstructural characterization (XRD, SEM, TEM, and N_2 adsorption) of the Na_2CO_3−ZrO_2 external shell produced during CO_2 chemisorption provided evidence for variations of some microstructural properties of the external shell as a function of temperature. Between 300 and 550 °C, the Na_2CO_3−ZrO_2 external shell possessed very interesting textural properties. The materials were mesoporous, and, consequently, the CO_2 chemisorption did not stop, even though the appropriate temperature to thermally activate diffusion processes had not been reached. On the other hand, if the CO_2 chemisorption process was produced at temperatures higher than 550 °C, the Na_2CO_3−ZrO_2 external shell sintered, which caused the mesoporosity to disappear. Under these thermal conditions, the CO_2 chemisorption was controlled by diffusion processes when the Na_2CO_3−ZrO_2 external shell covered the Na_2ZrO_3 particle surface.

These results confirmed the sintering process proposed in previous papers, which explained the atypical behavior observed in isothermal experiments. Nevertheless, in the previous studies, the sintering process had typically been attributed to the alkaline ceramic (the effect produced during the initial heating time). The results presented here suggest that the Na_2CO_3−ZrO_2 external shell was responsible for the microstructural changes observed.

AUTHOR INFORMATION

Corresponding Author

*Phone +52 (55) 5622 4627; Fax +52 (55) 5616 1371; E-mail pfeiffer@iim.unam.mx.

Notes

The authors declare no competing financial interest.

ACKNOWLEDGMENTS

This work was financially supported by CONACYT-SENER (150358). L. Martínez-dlCruz thanks CONACYT for personal financial support. The authors would like to thank to Adriana Tejeda, Carlos Flores, and Omar Novelo for technical help.

REFERENCES

(1) Choi, S.; Drese, J. H.; Jones, C. W. *ChemSusChem* **2009**, *2*, 796−854.
(2) Wang, Q.; Luo, J.; Zhong, Z.; Borgna, A. *Energy Environ. Sci* **2011**, *4*, 42−44.
(3) Yun-Hang, H., Ed. *Advances in CO_2 Conversion and Utilization*; ACS Symposium Series 1056; American Chemical Society: Washington DC, 2010.
(4) Drage, T. C.; Snape, C. E.; Stevens, L. A.; Wang, J. W.; Cooper, A. I.; Dawson, R.; Guo, X.; Satterley, C.; Irons, R. *J. Mater. Chem.* **2012**, *22*, 2815−2823.
(5) Reddy, E. P.; Smirniotis, P. G. *J. Phys. Chem. B* **2004**, *108*, 7794−7800.
(6) ÓAlessandro, D. M.; Smit, B.; Long, J. R. *Angew. Chem., Int. Ed.* **2010**, *49*, 6058−6082.
(7) Olivares-Marín, M.; Castro-Díaz, M.; Drage, T. C.; Maroto-Valerand, M. M. *Sep. Purif. Technol.* **2010**, *73*, 415−420.
(8) Essaki, K.; Muramatsu, T.; Kato, M. *Int. J. Hydrogen Energy* **2008**, *33*, 4555−4559.
(9) Yi, K. B.; Eriksen, D. Ø. *Sep. Sci. Technol.* **2006**, *41*, 283−290.
(10) Duan, Y. J. *Renewable Sustainable Energy* **2011**, *3*, 013102.
(11) Duan, Y.; Zhang, B.; Sorescu, D. C.; Johnson, J. K. *J. Solid State Chem.* **2011**, *184*, 304−311.

(12) Kang, S. Z.; Wu, T.; Li, X.; Mu, J. *Mater. Lett.* **2010**, *64*, 1404−1406.
(13) Essaki, K.; Kato, M. J. *Chem. Eng. Japan* **2006**, *39*, 1161−1164.
(14) Nair, B. N.; Burwood, R. P.; Goh, V. J.; Nakagawa, K.; Yamaguchi, T. *Prog. Mater. Sci.* **2009**, *54*, 511−541.
(15) Khomane, R. B.; Sharma, B.; Saha, S.; Kulkarni, B. D. *Chem. Eng. Sci.* **2006**, *61*, 3415−3418.
(16) Wang, K.; Guo, X.; Zhao, P.; Wang, F.; Zheng, C. *J. Hazard. Mater.* **2011**, *189*, 301−307.
(17) Rodríguez-Mosqueda, R.; Pfeiffer, H. *J. Phys. Chem. A* **2010**, *114*, 4535−4541.
(18) Korake, P. V.; Gaikwad, A. G. *Front. Chem. Eng. China* **2011**, *5*, 215−226.
(19) Yamaguchi, T.; Niitsuma, T.; Nair, B. N.; Nakagawa, K. *J. Membr. Sci.* **2007**, *294*, 16−21.
(20) Mejía-Trejo, V. L.; Fregoso-Israel, E.; Pfeiffer, H. *Chem. Mater.* **2008**, *20*, 7171−7176.
(21) López-Ortiz, A.; Perez-Rivera, N. G.; Reyes, A.; Lardizabal-Gutierrez, D. *Sep. Sci. Technol.* **2004**, *39*, 3559−3572.
(22) Khokhani, M.; Khomane, R. B.; Kulkarni, B. D. *J Sol-Gel Sci. Technol.* **2012**, *61*, 316−320.
(23) Alcérreca-Corte, I.; Fregoso-Israel, E.; Pfeiffer, H. *J. Phys. Chem. C* **2008**, *112*, 6520−6525.
(24) Zhao, T.; Ochoa-Fernández, E.; Rønning, M.; Chen, D. *Chem. Mater.* **2007**, *19*, 3294−3301.
(25) Pfeiffer, H.; Vazquez, C.; Lara, V. H.; Bosch, P. *Chem. Mater.* **2007**, *19*, 922−926.
(26) Ochoa-Fernandez, E.; Zhao, T.; Ronning, M.; Chen, D. *J. Environ. Eng.* **2009**, *37*, 397−402.
(27) Santillan-Reyes, G. G.; Pfeiffer, H. *Int. J. Greenhouse Gas Control* **2011**, *5*, 1624−1629.
(28) Ávalos-Rendón, T.; Casa-Madrid, J.; Pfeiffer, H. *J. Phys. Chem. A* **2009**, *113*, 6919−6923.
(29) Xiao, Q.; Liu, Y.; Zhong, Y.; Zhu, W. J. *Mater. Chem.* **2011**, *21*, 3838−3842.
(30) Yin, X. S.; Li, S. P.; Zhang, Q. H.; Yu, J. G. *J. Am. Ceram. Soc.* **2010**, *93*, 2837−2842.
(31) Iwan, A.; Stephenson, H.; Ketchie, W. C.; Lapkin, A. A. *Chem. Eng. J.* **2009**, *146*, 249−258.
(32) Yin, X. S.; Li, S. P.; Zhang, Q. H.; Yu, J. G. *Ind. Eng. Chem. Res.* **2010**, *49*, 6593−6598.
(33) Olivares-Marín, M.; Drage, T. C.; Maroto-Valer, M. M. *Int. J. Greenhouse Gas Control* **2010**, *4*, 623−629.
(34) Seggiani, M.; Puccini, M.; S. Vitolo, S. *Int. J. Greenhouse Gas Control* **2011**, *5*, 741−478.
(35) Yin, X. S.; Zhang, Q. H.; Yu, J. G. *Inorg. Chem.* **2011**, *7*, 2844−2850.
(36) Radfarnia, H. R.; Iliuta, M. C. *Ind. Eng. Chem. Res.* **2011**, *50*, 9295−9305.
(37) Xiao, Q.; Tang, X.; Liu, Y.; Zhong, Y.; Zhu, W. *Chem. Eng. J* **2011**, *174*, 231−235.
(38) Mosqueda, H. A.; Vazquez, C.; Bosch, P.; Pfeiffer, H. *Chem. Mater.* **2006**, *18*, 2307−2310.
(39) Lowell, S.; Shields, J. E.; Thomas, M. A. *Characterization of Porous Solids and Powders: Surface Area, Pore Size and Density*; Particle Technology Series; Kluwer Academic Publishers: London, 2004.
(40) McCash, E. M. *Surface Chemistry*; Oxford University Press: Oxford, U.K., 2002.
(41) Goldstein, J. I.; Newbury, D. E.; Echlin, P.; Joy, D. C.; Fiori, C.; Lifshin, E., *Scanning Electron Microscopy and X-ray Microanalysis*; Plenum: New York, 1981.